

Research Paper

Laboratory modelling of grouting in poorly-graded sand

W.C. Cheng¹, J.C. Ni² and S.L. Shen³

ARTICLE INFORMATION

Article history:

Received: 03 January, 2018

Received in revised form: 21 March, 2018

Accepted: 12 Desember, 2018

Publish on: 03 March, 2019

Keywords:

Hydrofracturing
Threshold seepage velocity
Fracture initiation pressure
Bleeding test

ABSTRACT

This paper presents a newly designed laboratory apparatus for grouting in poorly-graded sand. Sandy soil specimen was prepared by a wet-raining method. Bleeding tests were carried out to select a cement-bentonite mixture with minimal bleeding. Both water injection tests and grout injection tests were conducted to investigate the threshold seepage velocity, the fracture initiation pressure, and factors affecting the fracture initiation pressure using a plot of injection pressure (p) against injection rate (q). Under low q value, the development of p - q curve was not relevant to the overburden pressure applied and the p value was generally in a proportional linear relationship with the q value. It is also noted that for the same q value, the fracturing pressure required was increased with an increase in effective overburden pressure. Vertical oriented fractures were formed and then turned to a horizontal orientation. The subsequent turning of the fractures might be related either to the minimum compressive stress somehow being increased during the test or to the inhomogeneous nature of the sand specimen.

1 Introduction

Littlejohn (2003) defined permeation grouting as the application of low viscosity gelling solutions or particulate suspensions into the ground without disturbing nearby structures. The grout types and their material constituents are chosen so that they can flow without difficulty through the pores within the ground under relatively low injection pressures. Suspension grouts can be successfully injected into gravels and coarse sands. The use of very fine cement grouts for injection into fine to medium sands has been proposed to circumvent problems associated with the inability of ordinary cement grouts to permeate soil formations finer than coarse sand.

Hydraulic fracturing is a process which occurs when a fluid is injected into soil at a pressure which exceeds a threshold value, resulting in the initiation and propagation

of a thin fracture in the soil. Macroscopically, the failure mode for fracture initiation is considered to be either tensile or shear failure (Wong and Alfaro, 2001; Alfaro and Wong, 2001; Soga et al. 2005; 2006; Shen et al., 2003; Ni and Cheng, 2010a, 2010b, 2012a, 2012b; Marchi et al., 2013, Ni and Cheng, 2015). Due to a collapse of the Wei-Kuan building in the 6.4-magnitude earthquake in Tainan, Taiwan on 6th February 2016, improving the mechanical properties of the sandy foundation soils for existing buildings located in areas at high risk of liquefaction has become a priority for government authorities. Permeation grouting is deemed capable of increasing the strength and stiffness of ground. But poor field quality control could however lead to hydrofracturing of the soil. Laboratory testing can be utilised to characterise the injection pressure-rate relationship in this practice, and also to eliminate factors

¹ Corresponding author, State Key Laboratory of Ocean Engineering, School of Naval Architecture, Ocean, and Civil Engineering, Shanghai Jiao Tong University, Shanghai 200240, CHINA, s2428030@gmail.com

² Department of Civil Engineering, National Taipei University of Technology, Taipei 10608, Taiwan, R.O.C.

³ State Key Laboratory of Ocean Engineering, School of Naval Architecture, Ocean, and Civil Engineering, Shanghai Jiao Tong University, Shanghai 200240, CHINA.

Note: Discussion on this paper is open until September 2019

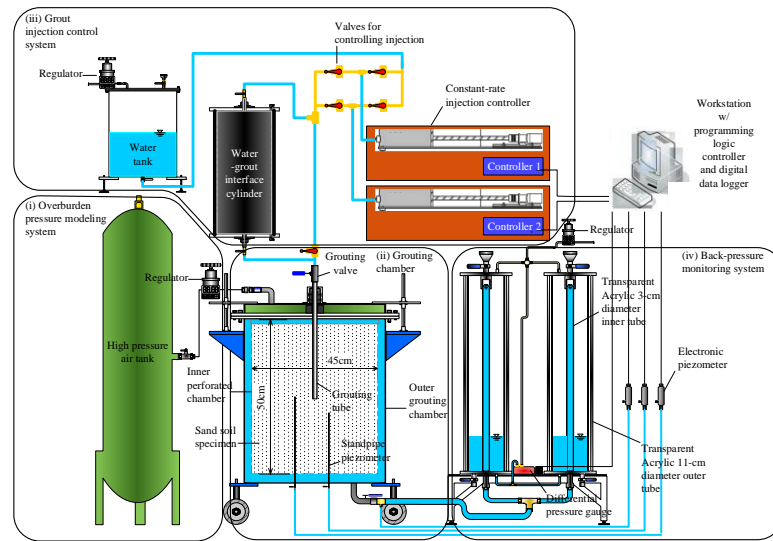


Fig. 1. Newly designed laboratory apparatus for the modeling of permeation grouting

that cannot be controlled in the field. This study aims: i) to develop a newly designed laboratory apparatus to better understand the characteristics of the injection pressure-rate relationship for permeation grouting, ii) to investigate the action of water and grout injection.

2 Laboratory apparatus

2.1 Newly designed laboratory apparatus

The laboratory apparatus developed in this study for modelling both the permeation grouting and the fracture grouting includes five major elements: i) an overburden pressure modelling system, ii) a grouting chamber, iii) a grout injection control system, iv) a back-pressure monitoring system, and v) a high-efficiency grout mixer, as shown in **Fig. 1**.

2.2 Calibration of injection pressure and rate

2.2.1 Calibration of injection pressure

Firstly, all the feed lines were de-aired. Secondly, the injection pressure (p) set by the programming logic controller was raised from 0 to 5 kg/cm² by increments of 0.5 kg/cm². The injection pressure (p) was then increased by increments of 1.0 kg/cm² until it reached 10 kg/cm². Thirdly, the fluid pressures (Y-axis) measured by manometers attached to the discharge lines were compared to the prescribed injection pressures (X-axis), as shown in **Fig. 2**.

2.2.2 Calibration of injection rate

As in injection rate calibration, all the feed lines were saturated at the first place. A 1000 ml volumetric cylinder was prepared, and the injection rate (q) was raised from 1 cm³/sec to 13 cm³/sec. The outflow volumes (Y-axis) measured from the volumetric cylinder were compared with the time duration (X-axis), as shown in **Fig. 3**.

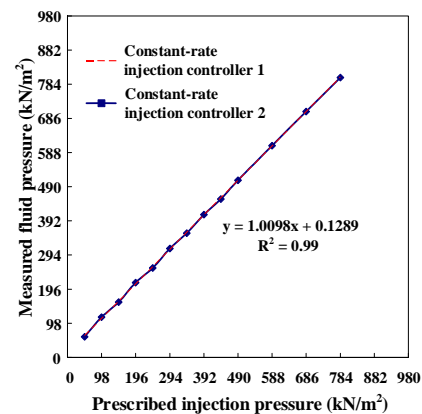


Fig. 2. Plot of the measured fluid pressure against the prescribed injection pressure

3 Grout used and injection experiment

A series of grout bleeding tests were carried out in accordance with ASTM C940-98a (1998), where the expansion and accumulation of bleed water at the

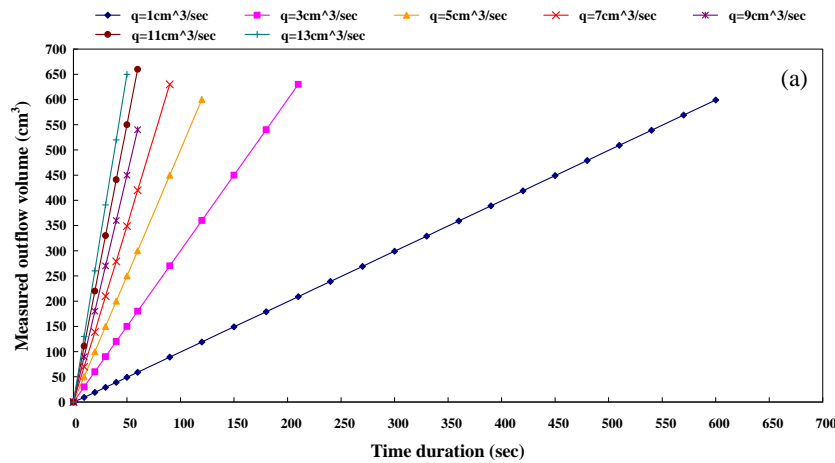


Fig. 3. Plot of the measured outflow volume against the time duration under a constant-rate injection controller.

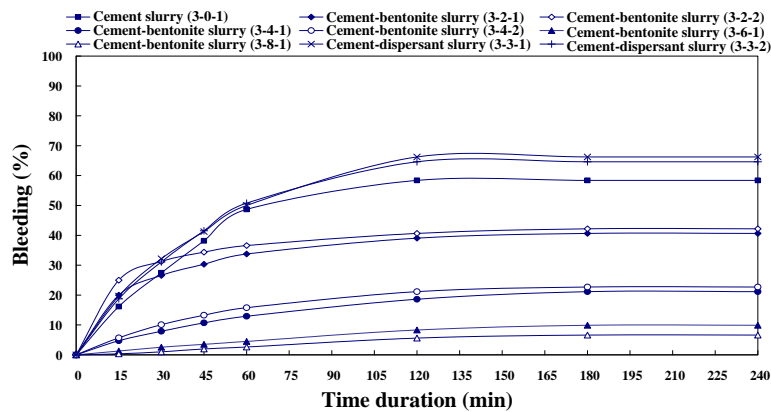


Fig. 4. Results of the bleeding tests (numbering description: water-cement ratio – addition of bentonite or dispersant – number of testing)

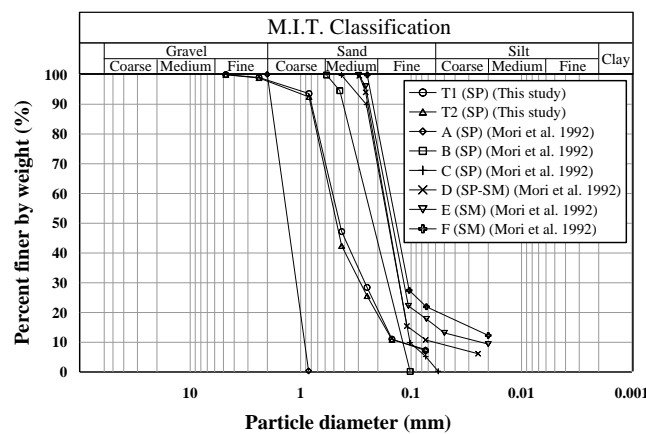


Fig. 5. Grading curves for the tested sandy soil

Table 1. Physical properties for the sand soil used in this study

Specific gravity (G_s)	Max dry unit weight $\gamma_{d,max}$ (g/cm^3)	Min dry unit weight $\gamma_{d,min}$ (g/cm^3)	D_{10} (mm)	D_{30} (mm)	D_{60} (mm)	Uniformity coefficient C_u	Curvature coefficient C_c	Soil type
2.69	1.65	1.44	0.14	0.25	0.52	3.71	0.86	SP

surface of the freshly mixed cement grout was measured at 15-minute intervals for the first 60 minutes, and thereafter at hourly intervals, until two successive readings showed no further expansion or bleeding. Portland cement Type 1 was the primary material used in the grouts. Grout mixtures were prepared with water-cement ratios of 3, 5, and 7. Some grouts had an addition of bentonite in the range of 2-8%. The bleedings varying with time for the grout mixtures are shown in **Fig. 4**.

The results indicate that the bleeding of grouts with a water-cement ratio of 3 was about 58.4%. By adding 2% bentonite, the bleeding of grouts at the same water-cement ratio was reduced to the range of 40.6-42.2%. The other three bleeding tests, on grouts with bentonite additions of 4-8%, showed that the greater the bentonite addition, the less the bleeding of grouts. In contrast, by adding 3% dispersant, the bleeding of grouts with a water-cement ratio of 3 was in the range of 66.3-64.6%, which is even higher than that for the grouts with a water-cement ratio of 3 without bentonite addition. Thus, minimum bleeding was obtained at 8% bentonite addition for the grouts with a water-cement ratio of 3.

The wet-raining method was adopted for preparing two sandy soil specimens, 45 cm in diameter and 50 cm in height. The grading curves for the tested sandy soil are shown in **Fig. 5**, while the soil physical properties are listed in Table 1. A 2-mm thick geotextile membrane was installed on the inner surface of the chamber. The sandy soil was then rained at a constant falling distance inside the inner perforated chamber. As the specimen raining was halfway complete, the grouting tube was positioned and lowered to a preset elevation 25 cm above the base. After the raining completed, a geotextile membrane of 43 cm in diameter was placed at the top of the specimen together with a load-carrying steel plate to ensure effective load transfer and upward drainage during grouting.

Specimen saturation was achieved by increasing the back-pressure to 343 kN/m² at steps of 49 kN/m². The effective overburden pressure was kept at a pressure 4.9 kN/m² higher than the back-pressure. To check the degree of saturation for specimens T1 and T2, the Skempton pore pressure parameter (B-value) was evaluated as 98% at specimen T1 and 96% at specimen T2 by introducing an additional overburden pressure of 49 kN/m². The water injection tests for specimens T1 and T2 were first carried out at effective overburden pressures of 49 kN/m² and 98 kN/m², respectively, and then the suspension grout prepared at a water-cement ratio of 3 and a bentonite addition of 8 % were injected into specimen T2 under an effective overburden pressure of 98 kN/m².

4 Results and analysis

4.1. Water injection test

4.1.1 Water injection activities

One of the benefits of introducing the newly designed laboratory apparatus is that the injection pressure can be measured by the built-in pressure gauge of the injection controller, by which the injection pressure-time curve can thus be produced. Water seepage through the soil specimen during injection will flow into the transparent inner tube and overflow to the annulus area between the two transparent tubes. This overflowing water will cause an elevation difference in the water column of the two transparent tubes, which can be sensed by the differential pressure gauge. The data from the differential pressure gauge can be used for producing the discharged volume-time curve. The porewater pressures measured from the two standpipe piezometers and the back-pressures of the specimen obtained through the three electronic piezometers are to produce the porewater pressure-time curves. The p value for the water injection activities of $q = 1 \text{ cm}^3/\text{sec}$ for sample T1 under $\sigma_v' = 49 \text{ kN/m}^2$ was stable at 345 kN/m² until the end of the injection test, representing that water seepage occurred at this very low injection rate. In the injection test of $q = 6 \text{ cm}^3/\text{sec}$, the p value measured at 353.8 kN/m² in the period of 1-3 min, and then declined to 343.9 kN/m², after which time the test was stopped and water was no longer injected (**Fig. 6a**). The p value for the water injection activities at $q = 1 \text{ cm}^3/\text{sec}$ for sample T1 under $\sigma_v' = 98 \text{ kN/m}^2$ measured at 347 kN/m² in the period of 0-17 min, after which time the test was stopped, implying that for $q = 1 \text{ cm}^3/\text{sec}$, penetration of water rather than hydrofracturing was occurred. As in the injection test of $q = 6 \text{ cm}^3/\text{sec}$, the p value was stable at 365.5 kN/m² in the period of 0-3 min and then dropped to 344.9 kN/m² (**Fig. 6b**). This pressure drop was most likely due to the hydrofracturing of the soil resulting from this faster injection of water. The p value measured at 354.8 kN/m² from 0 to 3 min, and then decreased to 343.0 kN/m² at $q = 6 \text{ cm}^3/\text{sec}$ for sample T2 under $\sigma_v' = 49 \text{ kN/m}^2$ (**Fig. 7a**). While it averaged 360.6 kN/m² from 0 to 2 min, and then declined to 342.0 kN/m² in the experiment at $q = 6 \text{ cm}^3/\text{sec}$ for the sample T2 under $\sigma_v' = 98 \text{ kN/m}^2$ (**Fig. 7b**). These two pressure declines were ascribed to a response to the initiation of hydrofracturing of the sandy soil as the water injection rate was greater than the threshold seepage velocity.

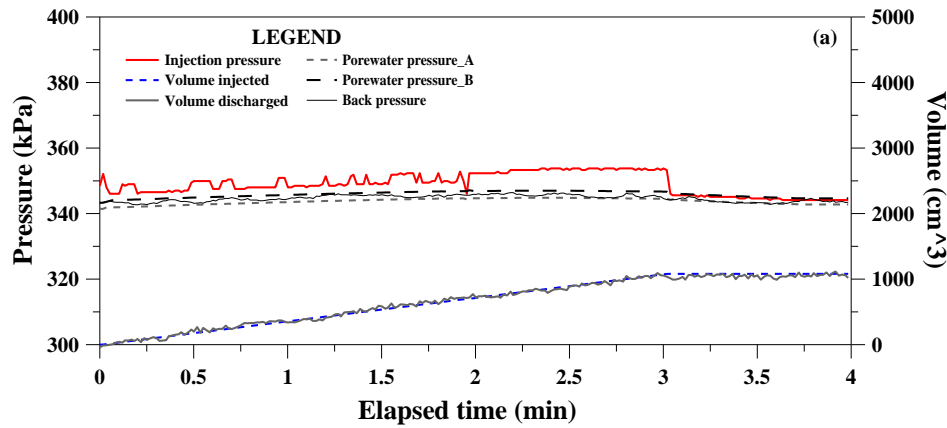


Fig. 6. Injection pressure-rate relationship from the water injection experiment of sample T1 at $\sigma_v' = 49 \text{ kN/m}^2$ ($q = 6 \text{ cm}^3/\text{sec}$)

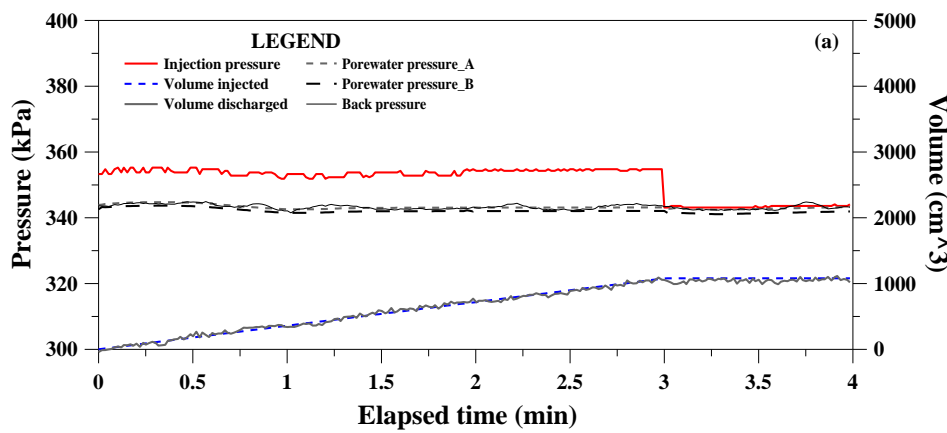


Fig. 7. Injection pressure-rate relationship from the water injection experiment of sample T2 at $\sigma_v' = 49 \text{ kN/m}^2$ ($q = 6 \text{ cm}^3/\text{sec}$)

4.1.2 Threshold seepage velocity

The critical hydraulic gradient (i_c) is first calculated as 6.74 through the permeability of sand, $k = 0.0055 \text{ cm/sec}$, using Eq. (1) which is widely used for determining the i_c value in local engineering practice. Then the threshold seepage velocity can be determined to be 0.088 cm/sec using Eqs. (2) and (3), taking the void ratio of sand as $e = 0.73$ into account. It has been found from several trial calculations that the water injection rate of $q = 6 \text{ cm}^3/\text{sec}$ across a gross unit area of 68.2 cm^2 (i.e., the area penetrated by the water) is approximately equal to the threshold seepage velocity of 0.088 cm/sec , thereby leading to the hydrofracturing of soil.

$$i_c = 1 / (2 \times \sqrt{k}) \quad [1]$$

$$v = k \times i_c \quad [2]$$

$$v_s = v \times (1 + e) / e \quad [3]$$

4.1.3 Determination of P_{frac} value

For the q value range of $1\text{-}5 \text{ cm}^3/\text{sec}$, the p - q curves for sample T1 under $\sigma_v' = 49 \text{ kN/m}^2$ are comparable with those for sample T1 under $\sigma_v' = 98 \text{ kN/m}^2$ (Fig. 8a). This fact can also be seen for those p - q curves from sample T2 (Fig. 8b), implying that for lower q values, the development of the p - q curve is not relevant to the applied overburden pressure. As in the range of $q = 1\text{-}5 \text{ cm}^3/\text{sec}$, the p value was generally in a proportional linear relationship with the q value. The p value for sample T1 under $\sigma_v' = 49 \text{ kN/m}^2$ declined from 353.8 kN/m^2 at $q = 6 \text{ cm}^3/\text{sec}$ to 348.4 kN/m^2 at $q = 7 \text{ cm}^3/\text{sec}$, indicating that the initiation of hydrofracturing of the sand occurred as the q value reached $6 \text{ cm}^3/\text{sec}$, and the p value of 353.8 kN/m^2 was the corresponding fracturing pressure (P_{frac}). The P_{frac} value of 365.5 kN/m^2 for sample T1 under $\sigma_v' = 98 \text{ kN/m}^2$ was noted as the q value increased to $6 \text{ cm}^3/\text{sec}$, which is greater than the P_{frac} value of 353.8 kN/m^2 for sample T1 under $\sigma_v' = 49 \text{ kN/m}^2$.

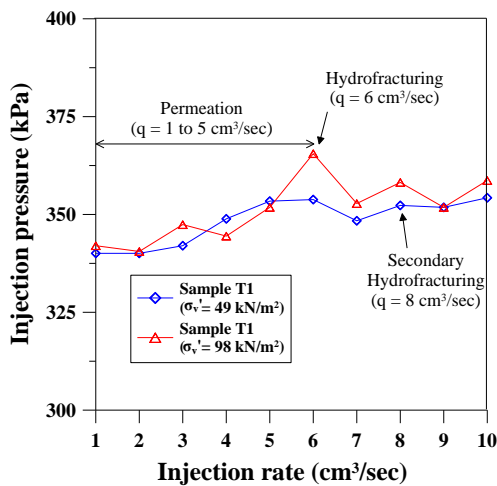


Fig. 8. Injection pressure-rate activities in the water injection test

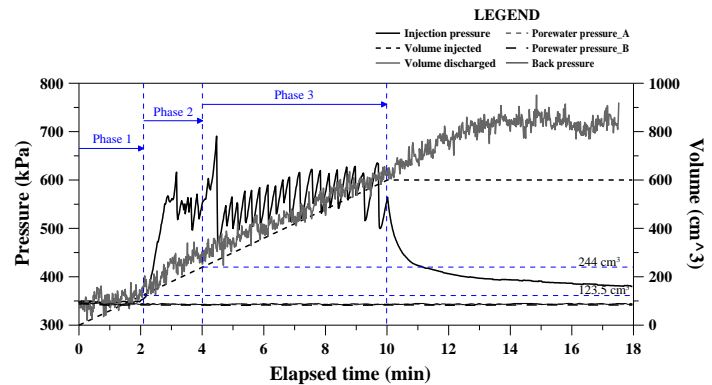


Fig. 9. Relationship between injection pressure, volume injected, volume discharged, porewater pressure, and back-pressure from the grout injection experiment of sample T2 at $\sigma_v' = 98 \text{ kN/m}^2$ ($q = 1 \text{ cm}^3/\text{sec}$)

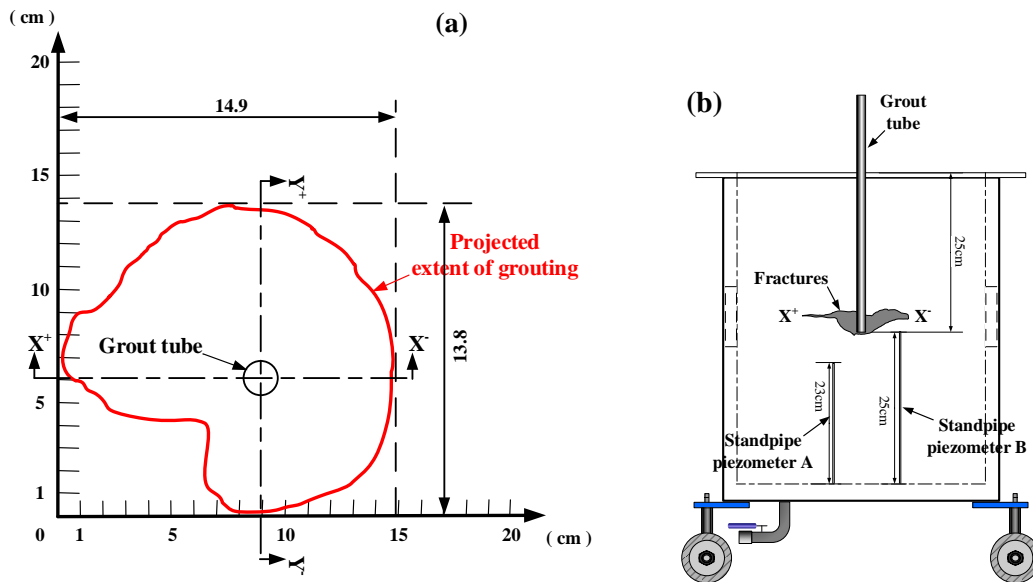


Fig. 10. Mapping result of the fractures: (a) Plan view (b) x-dir mapping result

4.2 Grout injection test

This fact can also be seen from the test results from sample T2. The greater the effective overburden pressure, the higher the fracturing pressure required for the same injection rate.

4.2.1 Grout injection activities

It can be seen from **Fig. 9** that as friction between the grout and the pipeline was deemed negligible, the injection pressure initially showed little change and the consumed volume of grout in the pipeline from the water-grout interface cylinder to the grouting valve was about

123.5 cm^3 (see “Phase 1” in **Fig. 9**). Then the injection pressure increased to 616.4 kN/m^2 as the grout flowed through a right-angle pipeline to grout tube connector (see “Phase 2” in **Fig. 9**). The injection pressure was stable at the range of 522.3-567.4 kN/m^2 from 3.2 to 4 min. The consumed volume of grout from 2 to 4 min was increased by 120.5 cm^3 to 244 cm^3 . As the grout was injected into the specimen, the injection pressure increased dramatically to 690.9 kN/m^2 and then dropped to 476.3 kN/m^2 where the specimen was fractured by the grout despite the small q value (see “Phase 3” in **Fig. 9**). The injection pressure due to the grout viscosity and pipeline friction averaged 476 kN/m^2 from 4.5 to 10 min. The actual grout take from 4 to 10 min was estimated to be 356 cm^3 ($600 \text{ cm}^3 - 244 \text{ cm}^3$).

4.2.2 Determination of P_{frac} value

The grout started to be injected into the specimen after the grout take reached 244 cm³ at 4 min after the start of grout injection. Thus, the injection pressure-time curve between 4 and 10 min can be used for determining the p_{frac} value. It can be seen from Fig. 10 that the maximum p value was 690.9 kN/m² and that the p value from "Phase 2" where the grout had not yet reached the specimen was in the range of 522.3-567.4 kN/m². By deducting the back-pressure of 343 kN/m² from the p value of 567.4 kN/m², the increase in the p value due to pipeline friction can be calculated to be 224.4 kN/m². The p_{frac} value can thus be determined as 466.5 kN/m². In the case where the pipeline friction-induced pressure increase is omitted, the p_{frac} value of 690.9 kN/m² is close to that from sample C in the tests by Mori et al. (1992).

4.2.3 Initiation and propagation of fractures

In the tests, the sandy soil was K_0 -consolidated to the required stress state. Fig. 10 shows the mapping result of the fractures. As can be seen, the projected extent of grouting averaged 14.4 cm and the fractures were not uniformly developed. The inhomogeneous nature of the sand specimen might play an important role in this phenomenon. It can also be seen from Fig. 10 that the fractures initiated with a vertical orientation and then turned to a horizontal orientation. The fracture orientation was initially perpendicular to the direction of the minimum compressive stress. The subsequent turning of the fractures to the horizontal orientation might be related to either the horizontal compressive stress apparently being increased during the experiment or the inhomogeneous nature of the specimen.

5 Conclusions

Based on the results of the water and grout injection tests, the following conclusions can be drawn:

(1) The p value from the water injection test generally increases linearly with an increasing q value prior to the hydrofracturing of the sandy soil. Where the q value is lower than the threshold seepage velocity, the p - q curve for a sample with a lower σ_v' is comparable with that for a sample with a higher σ_v' . In cases where the same q value is adopted, the p_{frac} increases with an increasing σ_v' .

(2) The p_{frac} value obtained from the grout injection test was close to that from sample C in the tests by Mori et al. (1992). Vertical oriented fractures were formed

initially, and these then turned to a horizontal orientation. The subsequent turning of the fractures might be related either to the minimum compressive stress somehow being increased during the test or to the inhomogeneous nature of the specimen.

(3) The threshold seepage velocity and the fracture initiation pressure should be assessed through the characteristics of the p - q curve suggested in this paper, using a series of modelled p - q curves for different overburden pressures. Trial grouting is needed to verify the accuracy of the obtained results to prevent the hydrofracturing of the soil during field grouting.

Acknowledgements

This study would not have been possible without the financial support from the National Science Council of Taiwan under the Contract No. NSC97-2622-E-027-013-CC3.

References

- Alfaro, M.C. and Wong, R.C.K., 2001. Laboratory studies on fracturing of low-permeability soils. *Canadian Geotechnical Journal*, **38**: 303–315.
- ASTM, 1998. Standard Test Method for Expansion and Bleeding of Freshly Mixed Grouts for Preplaced-Aggregate Concrete in the Laboratory C940-98a. West Conshohocken, PA: ASTM International.
- Littlejohn, S., 2003. The Development of Practice in Permeation and Compensation Grouting: A Historical Review (1802-2002). *Grouting and Ground Treatment*. New Orleans, Louisiana: American Society of Civil Engineers.
- Mori, A., Tamura, M., Shibata, H. and Hayashi, H., 1992. Some factors related to injected shape in grouting. In: *Grouting, Soil Improvement and Geosynthetics*, GSP 30. New York: ASCE, 313-324.
- Ni, J.C. and Cheng, W.C., 2010a. Monitoring and modeling grout efficiency of lifting structure in soft clay. *International Journal of Geomechanics*, **10**(6): 223-229.
- Ni, J.C. and Cheng, W.C., 2010b. Using fracture grouting to lift structures in clayey sand. *Journal of Zhejiang University – SCIENCE A*, **11**(11): 879-886.
- Ni, J.C. and Cheng, W.C., 2012a. Trial grouting under rigid pavement: A case history in Magong Airport, Penghu. *Journal of Testing and Evaluation*, **40**(1): 1-12.
- Ni, J.C. and Cheng, W.C., 2012b. Characterising the failure pattern of a station box of Taipei Rapid Transit System (TRTS) and its rehabilitation. *Tunnelling and Underground Space Technology*, **32**: 260-272.

- Marchi, M., Gottardi, G. and Soga, K., 2013. Fracturing pressure in clay. *Journal of Geotechnical and Geoenvironmental Engineering*, **140**(2): 1-9.
- Ni, J.C. and Cheng, W.C., 2015. Field response of high speed rail box tunnel during horizontal grouting. *Journal of Testing and Evaluation*. **43**(2): 1-16.
- Shen, S.L., Miura, N. and Koga, H., 2003. Interaction mechanism between deep mixing column and surrounding clay during installation. *Canadian Geotechnical Journal*, **40**(2): 293–307.
- Soga, K., Ng, M.Y.A. and Gafar, K., 2005. Soil fractures in grouting. *Proceedings of the 11th International congress on Computer Methods and Advances in Geomechanics*; Turin, Italy.
- Soga, K., Gafar, K., Ng, M.Y.A. and Au, S.K.A., 2006. Macro and micro behaviour of soil fracturing. *Proceedings of the International Symposium on Geomechanics and Geotechnics of Particulate Media*, Yamaguchi.
- Wong, R.C.K. and Alfaro, M.C., 2001. Fracturing in low-permeability soils for remediation of contaminated ground. *Canadian Geotechnical Journal*, **38**: 316–327.